Quantum walks and quantum simulations with Bloch-oscillating spinor atoms

D. Witthaut

QUANTOP, The Niels Bohr Institute, University of Copenhagen, DK-2100 Copenhagen, Denmark and Network Dynamics Group,
Max-Planck-Institute for Dynamics and Self-Organization, D-37073 Göttingen, Germany

We propose a scheme for the realization of a quantum walker and a quantum simulator for the Dirac equation with ultracold spinor atoms in driven optical lattices. A precise control of the dynamics of the atomic matter wave can be realized using time-dependent external forces. If the force depends on the spin state of the atoms, the dynamics will entangle the inner and outer degrees of freedom, which offers unique opportunities for quantum information and quantum simulation. Here we introduce a method to realize a quantum walker based on the state-dependent transport of spinor atoms and a coherent driving of the internal state. In the limit of weak driving the dynamics are equivalent to that of a Dirac particle in $1 + 1$ dimensions. Thus it becomes possible to simulate relativistic effects such as Zitterbewegung and Klein tunneling.

I. INTRODUCTION

Quantum simulators aim at the simulation of complex quantum systems in well-controllable laboratory experiments [1]. Such a simulation is especially useful when the original quantum system is experimentally not accessible and classical simulations are impossible due to the exponential size of the Hilbert space. Furthermore, quantum simulators offer the possibility to tune the experimental parameters to explore novel physical phenomena. Important examples include the simulation of solid state systems with ultracold atoms [2], Dirac dynamics with graphene [3,4] or trapped ions [5,6], and sonic black holes in Bose-Einstein condensates [7].

Ultracold atoms in optical lattices are especially suited for such a task since their dynamics can be controlled with an astonishing precision and their dynamics can be measured *in situ*. In the present paper we propose to use spinor atoms in tilted or driven optical lattices to realize a quantum walker—a paradigmatic system in quantum information science [8–12]—and a quantum simulator for relativistic Dirac dynamics. In contrast to previous proposals which were based on the realization of artificial gauge fields using atoms with a tripod internal structure [13,14], we focus on simple spinor atoms with two internal states, which are used routinely in ongoing experiments. The necessary correlations between the internal and the external dynamics can be realized with state-dependent external forces, in particular, by magnetic gradient fields [15–19]. Using a suitable driving of this external field and microwave transitions between the internal states [20,21], one can obtain control over the full dynamics of the atoms.

II. BLOCH OSCILLATIONS AND TRANSPORT IN OPTICAL LATTICES

A Bloch oscillation is the counterintuitive dynamic of a quantum particle in a periodic potential subject to a static external force. The force accelerates the particle until it reaches the edge of the Brillouin zone, where it is Bragg reflected. If Landau-Zener tunneling to higher bands can be neglected, this leads to a fully periodic motion. This peculiar kind of dynamic was postulated by Bloch already in 1928 in the context of electrons in crystals [22] but never observed

because of the strong scattering of the electrons. Thus it took another seven decades before Bloch oscillations could be demonstrated for electrons in semiconductor superlattices [23], photons in waveguide arrays [24], and ultracold atoms in optical lattices [25]. The latter realization especially shows an astonishing level of coherence and offers various possibilities to precisely control the atomic dynamics. Recent experiments have demonstrated that Bloch oscillations can persist over tens of thousand of periods and extend over macroscopic distances [17]. An example of Bloch oscillations of an atomic matter wave is shown in Fig. 1(a).

Extensive possibilities to control the atomic motion can be realized in driven optical lattices (i.e., in lattices with a time-dependent external field [15,26–31]). A particular interesting case is periodic driving, when the direction of the field is reversed before the matter wave reaches the edge of the Brillouin zone, decelerating the wave packet back to a standstill. Thus the atoms always have a positive momentum such that directed transport is realized, as illustrated in Fig. 1(b) for a sinusoidal driving.

To be precise, we have simulated the dynamics of ultracold Cs atoms in an optical lattice with a wavelength of $\lambda = 1064$ nm and a depth of $V_0 = E_R$. The strength of the external field was assumed to be $F_0/m = 0.42$ m/s^2, which can be easily realized by accelerating the optical lattice [25] or by a magnetic gradient field [15,17]. The dynamics of the atomic matter wave is then given by the Wannier-Stark Hamiltonian

$$\hat{H}(t) = \frac{-\hbar^2}{2m}\frac{\partial^2}{\partial x^2} + V_0\cos^2(k_0 x) + F(t)x, \qquad (1)$$

where $k_0 = 2\pi/\lambda$ and $E_R = \hbar^2 k_0^2/2m$ is the atomic recoil energy. The initial state has been chosen as a Bloch state with zero momentum weighted by a Gaussian with a width $\sigma = 6\lambda$. For a static field one then finds the celebrated Bloch oscillations with a period given by the Bloch time $T_B = 4\pi\hbar/\lambda F_0$. The maximum displacement of the wave packet is given by $d = \Delta/F_0$, Δ being the width of the ground Bloch band [26].

A directed transport of the atoms can be realized by means of a time-periodic driving. During one period of the driving the atoms are first accelerated and the decelerated back to a standstill, such that the atomic wave function is displaced
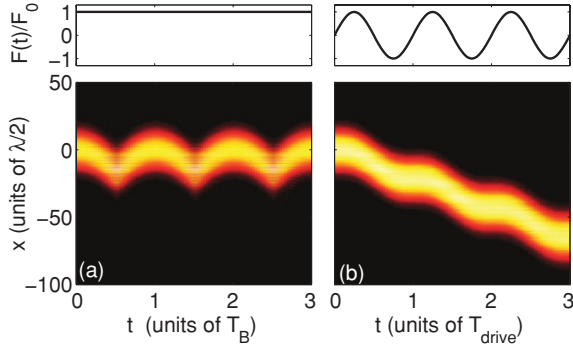
FIG. 1. (Color online) Dynamics of ultracold Cesium atoms in a driven optical lattice. (a) A static external field leads to Bloch oscillations. (b) A sinusoidal driving of the field leads to directed transport. We assumed an optical lattice with a wave length $\lambda = 1064$ nm, a depth of $V_0 = E_R$ and a maximum field strength of $F_0/m = 0.42$ m/s^2. The time is given in units of the Bloch period $T_B = 8.44$ ms and the period of the external driving $T_{\rm drive} = 10$ ms, respectively.

in space but otherwise unaffected. An example for directed transport in a driven optical lattice is shown in Fig. 1(b) for a sinusoidal driving

$$F(t) = F_1 \cos(2\pi t/T), \tag{2}$$

assuming a driving strength of $F_1/m = 0.42$ m/s^2 with a period of $T = 10$ ms. The transport properties of a driven optical lattice can be calculated analytically within the tight-binding approximation [26,27]. It is found that transport is possible only for a pure ac driving, while it is generally forbidden in the case of a combined dc and ac field $F(t)$ except for the case of a resonant driving $T = nT_B$. The actual transport velocity depends on the initial state, but an upper bound can easily be found

$$v_{\rm max} = \frac{d\Delta}{2\hbar} J_n \left(\frac{dF_1}{\hbar\omega} \right), \tag{3}$$

where J_n is an ordinary Bessel function. The case of a pure ac driving corresponds to $n = 0$. The dispersion of a wave packet is generally negligible for an initially broad wave packet as it vanishes with $1/\sigma^4$ [15,27,28]. This approach to controlling transport in driven optical lattices was experimentally demonstrated in [30,31].

III. QUANTUM WALKS

Now consider the dynamics of a spinor atom, where the atoms experience a different field strength depending on their initial state. Using Bloch oscillations and the directed transport described previously, it is possible to entangle the position and the internal degrees of freedom. This provides the basis for the implementation of a quantum walk or a Dirac quantum simulator.

One possibility to induce a state-dependent transport of spinor atoms is the use of a magnetic gradient field. In particular, we consider the dynamics of ultracold Cs atoms with the internal states $|\uparrow\rangle = |F = 4, m_F = 4\rangle$ and $|\downarrow\rangle = |F = 3, m_F = 3\rangle$ [16]. The magnetic moments of these two internal states are opposite, such that they move into different

directions in a magnetic gradient field. The effective potential is given by

$$V_{m_F}(x) = g_F m_F \mu_B \Delta B x, \tag{4}$$

assuming a linear magnetic gradient field $B_z(x) = \Delta B x$. The effective Landé factor of the two internal states is given by $g_{F=4} = 1/4$ and $g_{F=3} = -1/4$ [32] and $\mu_B = 9.274 \times 10^{-24}$ J/T denotes the Bohr magneton. The magnetic gradient field can also be varied in time to control the atomic motion [15]. Furthermore, we assume that the internal state of the atoms can be manipulated coherently by resonant microwave pulses with Rabi frequency $\Omega(t)$ [20]. The dynamics of the atomic state $[\psi_\uparrow(x,t), \psi_\downarrow(x,t)]$ is thus given by the Hamiltonian

$$\hat{H}(t) = \frac{-\hbar^2}{2m} \frac{\partial^2}{\partial x^2} + V_0 \cos^2(k_0 x)$$
$$+ \begin{pmatrix} V_\uparrow(x) & 0 \\ 0 & V_\downarrow(x) \end{pmatrix} + \frac{\hbar\Omega(t)}{2} \hat{\sigma}_x. \tag{5}$$

A coherent quantum walker can be implemented by a sinusoidal driving of the gradient field $\Delta B(t) = \Delta B_0 \times \sin(2\pi t/T)$. During one period, the atoms are first accelerated and then decelerated back to a standstill as illustrated in Fig. 1(b). However, the transport direction depends on the direction of the external field, which is opposite for both internal states, thus realizing an effective quantum walk. The coin operation is then realized by a $\pi/2$ pulse coupling the two hyperfine levels after integer multiples of the driving time T. An example of a quantum walk is shown in Fig. 2(c), where we have plotted the dynamics of the complete atomic density $|\psi_\uparrow(x,t)|^2 + |\psi_\downarrow(x,t)|^2$. The time dependence of the magnetic gradient field and the microwave pulses are illustrated in the upper panels of the figure. Initially, all atoms are assumed to be in the internal state $|\downarrow\rangle \otimes \psi_0(x)$, where the spatial wave function $\psi_0(x)$ is a Bloch state with $\kappa = 0$, weighted with a
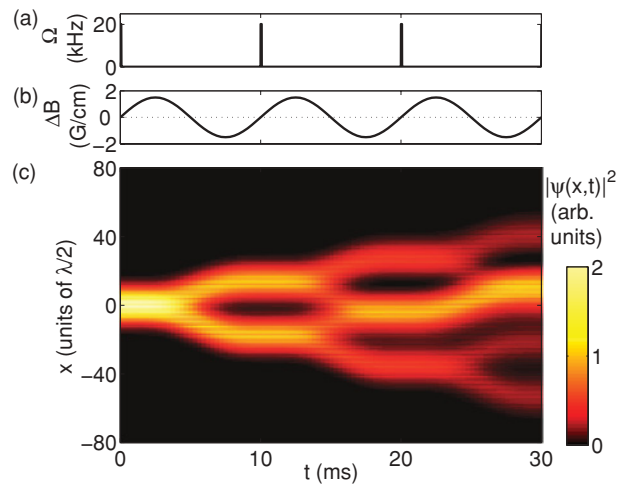

FIG. 2. (Color online) Quantum walk of ultracold Cs atoms in a driven magnetic gradient field. (a) The coin operations: Rabi frequency of the microwave $\pi/2$ pulses inducing transitions between the two hyperfine levels. (b) The shift operation: A driven magnetic gradient field induces state-dependent transport. (c) The resulting dynamics of the total atomic density $|\psi_\uparrow(x,t)|^2 + |\psi_\downarrow(x,t)|^2$. Parameters are given in the text.
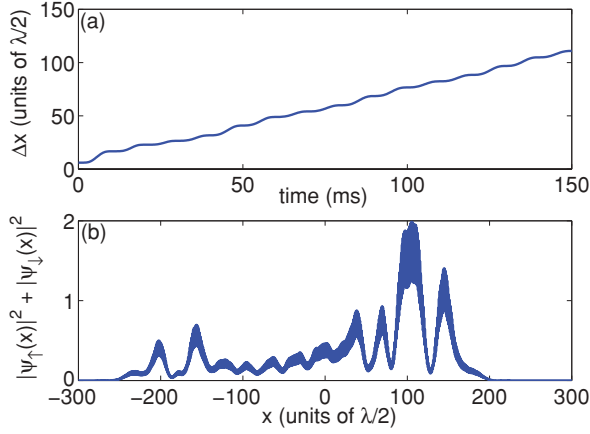
FIG. 3. (Color online) Characterization of a Bloch quantum walk. (a) Increase of the standard deviation $\Delta x = \sqrt{\langle x^2 \rangle - \langle x \rangle^2}$. (b) The total atomic population $|\psi_\uparrow(x,t)|^2 + |\psi_\downarrow(x,t)|^2$ after 15 driving periods. The parameters are given in the text.

Gaussian envelope of width $\sigma = 3\lambda$. The depth of the optical lattice is given by $V_0 = E_R$. The Bloch quantum walk is further analyzed in Fig. 3, where the width of the atomic wave packet $\Delta x(t)$ and the final atomic density are plotted. A quantum walk is characterized by a linear increase of the width $\Delta x \sim t$ in contrast to a classical random walk for which $\Delta x \sim t^{1/2}$.

It has to be noted that the magnitude of the force is different for the two spin states leading to a trivial overall displacement of the atomic density pattern. Furthermore this introduces a phase shift between the two spinor components, which has more severe consequences. This phase shift can be avoided by choosing internal states with the same m_F (i.e. $|\uparrow\rangle = |4,3\rangle$ instead of $|4,4\rangle$) or it can be compensated actively by a static magnetic field.

IV. DIRAC DYNAMICS

For weak driving, the dynamics of a quantum walker are equivalent to that of a Dirac particle in the $1 + 1$ dimension [33], which can be seen as follows. During one period T the atoms are first displaced depending on their internal state and then the internal state is rotated by an angle θ. Assuming that the internal rotation is fast compared to T, the dynamics are given by the evolution operator $\hat{U}(nT) = (\hat{U}_2 \hat{U}_1)^n$ with

$$\hat{U}_1 = \begin{pmatrix} \hat{D}_d & 0 \\ 0 & \hat{D}_{-d} \end{pmatrix} \quad \text{and} \quad \hat{U}_2 = \exp(-i\theta\hat{\sigma}_x/2), \quad (6)$$

where $\hat{D}_d$ denotes the translation operator over a distance d. In the limit of weak driving (i.e., small values of d and θ) the dynamics can be described by an effective Hamiltonian $\hat{U}(nT) \approx \exp(-i\hat{H}_{\text{eff}}n)$, which is given by

$$\hat{H}_{\text{eff}} = d\hat{p}\hat{\sigma}_z + \frac{\theta}{2}\hat{\sigma}_x. \quad (7)$$

This is just the Dirac Hamiltonian with an effective mass $m = \theta/2d$ and the momentum operator $\hat{p} = -i\partial/\partial x$.

According to these results, ultracold spinor atoms show an effective relativistic dynamics if the displacement d and the rotation angle θ are reduced. This is simply realized by increasing the lattice depth V_0 and decreasing the strength of
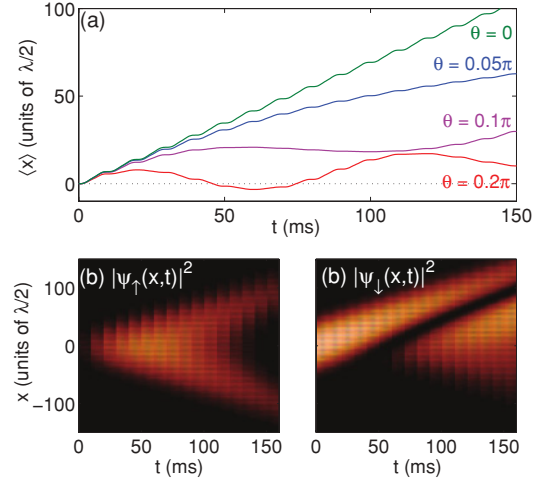

FIG. 4. (Color online) Zitterbewegung of spinor atoms in a driven magnetic gradient field. (a) Evolution of the position expectation value for different values of the rotation angle θ. (b) and (c) Evolution of the probability densities $|\psi_\uparrow(x,t)|^2$ and $|\psi_\downarrow(x,t)|^2$ for $\theta = 0.1\pi$. The remaining parameters are given in the text.

the microwave driving field. An example is shown in Fig. 4 for atoms initially prepared in the internal state $|\downarrow\rangle = |3,3\rangle$ with a width $\sigma = 10\lambda$. The optical lattice is now deeper as in the previous examples, $V_0 = 5E_R$. Transitions to the other spin state $|\uparrow\rangle = |4,3\rangle$ are induced at integer multiples of the period T_{drive} with a variable rotation angle $\theta = \Omega t_{\text{pulse}}$. For $\theta = 0$, the internal state does not change such that the atoms are steadily transported by the time-periodic external force. Increasing θ and thus the effective mass of the Dirac particle leads to a Zitterbewegung of the atoms, which is illustrated in Fig. 4(a). As expected, the period of the oscillations decreases with the effective mass m. Microscopically, the oscillations of the position expectation value $\langle x(t) \rangle$ result from the interference of the two components of the atomic state, which are shown in Figs. 4(b) and 4(c).

One of the most surprising predictions of Dirac theory is the Klein paradox: Relativistic particles are not repelled by a strong repulsive potential, but perfectly transmitted if the height of the potential step exceeds $2mc^2$ [34]. Signatures of this effect can be readily explored with ultracold atoms in driven optical lattices. We consider a situation where an additional blue detuned top-hat laser beam is focused aside of the atom cloud. We model the induced optical dipole potential by a tanh profile such that the total optical potential is given by

$$V(x) = V_{\text{lattice}}(x) + V_{\text{step}}(x)$$
$$= V_0 \cos^2(k_0 x) + \frac{V_s}{2}\{\tanh[(x - x_s)/w] + 1\}. \quad (8)$$

If the additional potential is weak enough, the directed transport mechanism remains mostly unaffected. However, the atomic wave packets accumulate a dynamical phase depending on their position, which is equivalent to a potential in the effective Dirac Hamiltonian (7). In this regime, the dynamics are described by the discrete evolution operator

$$\hat{U}(nT) \approx (\hat{U}_3 \hat{U}_2 \hat{U}_1)^n \quad \text{with}$$
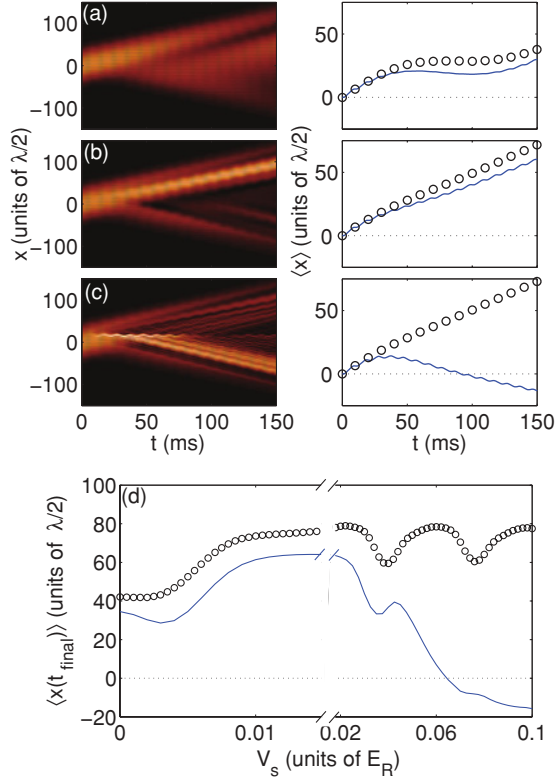$$\hat{U}_3(x) = \exp[-i V_{\text{step}}(x)T/\hbar], \quad (9)$$

FIG. 5. (Color online) Dynamics of spinor atoms in the Dirac regime with an additional potential step. (a)–(c) Evolution of the atomic density (left) and the position expectation value $\langle x(t)\rangle$ (right) for different heights of the potential step: (a) $V_{\text{step}}/E_R = 0$, (b) 0.015, and (c) 0.1. (d) Position expectation value $\langle x(t)\rangle$ after a fixed propagation time $t_{\text{final}} = 150$ ms as a function of the potential step V_s. Results of a full quantum simulation (solid blue line) are compared to the effective discrete Dirac approximation (open circles). The remaining parameters are the same as in Fig. 4 with $\theta = 0.1\pi$.

and $\hat{U}_{1,2}$ given in Eq. (6). The dynamics in the presence of an additional potential are shown in Fig. 5, comparing a full simulation to the Dirac approximation (9). A good agreement is observed for weak potential steps $V_s \lesssim 0.02 E_R$.

A pronounced signature of the Klein tunneling observed in Fig. 5 is that the repulsive potential step *enhances* the transmission of the atomic matter wave. Without the potential, the atoms exibit a Zitterbewegung as discussed previously. If a weak additional potential step is included (e.g., $V_s = 0.015 E_R$) the oscillating motion is gone and the atoms move steadily above the barrier. An even stronger potential, however, suppresses the directed transport underlying the Dirac quantum simulator. The effective description by the Dirac Hamiltonian (7) is no longer appropriate and the atoms are reflected just like ordinary Schrödinger particles. In this regime the Dirac approximation clearly deviates from the exact simulation results.

V. DECOHERENCE

Real experiments with spinor atoms are limited by a loss of coherence due a coupling to the environment. The schemes discussed previously make use on the opposite magnetic
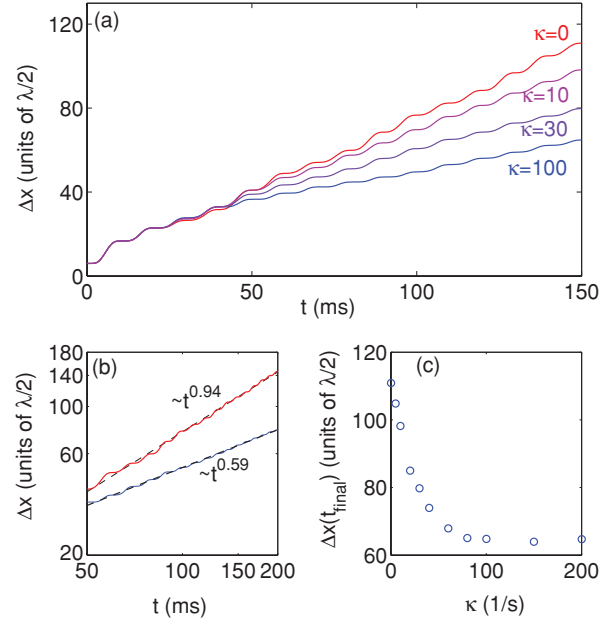

FIG. 6. (Color online) Quantum walk in the presence of decoherence. (a) Increase of the standard deviation $\Delta x(t)$ for different values of the dephasing rate κ. (b) The standard deviation in a loglog plot showing a different scaling $\Delta x(t) \sim t^\alpha$ in the quantum regime ($\kappa = 0$) and in the classical regime ($\kappa = 100$ s^{-1}). The dashed black line is a linear fit with the result $\alpha = 0.94$ and $\alpha = 0.59$, respectively. (c) The standard deviation $\Delta x(t_{\text{final}})$ after a fixed time $t_{\text{final}} = 150$ ms as a function of κ.

moment of the two hyperfine states $|\uparrow\rangle$ and $|\downarrow\rangle$ to transport the atoms in different directions. However, this makes the atomic state vulnerable to dephasing caused by magnetic-field fluctuations [9], while spatial coherence can be conserved over seconds [17]. To explore the effects of decoherence, we simulate the dynamics in the presence of pure dephasing described by the Master equation

$$\frac{\partial \hat{\rho}}{\partial t} = -\frac{i}{\hbar}[\hat{H}, \hat{\rho}] - \frac{\kappa}{2}\left(\hat{\sigma}_z^2 \hat{\rho} + \hat{\rho}\hat{\sigma}_z^2 - 2\hat{\sigma}_z\hat{\rho}\hat{\sigma}_z\right). \quad (10)$$

For the numerical calculations we use the quantum jump method [35], averaging over 100 trajectories.

Decoherence of the atomic states essentially turns a quantum random walk into a classical one, which is confirmed by the simulations shown in Fig. 6. After a short initial period the standard deviation Δx grows much slower in the the presence of dephasing. The linear increase $\Delta x(t) \sim t$ gradually changes into the classical diffusion law $\Delta x(t) \sim t^{1/2}$ if κ is increased. The different scaling is analyzed quantitatively in part (b), where $\Delta x(t)$ is plotted on a log-log scale together with a linear fit, omitting the initial expansion of the atomic matter wave. The different slope of the two curves directly reveals the different diffusion exponents. The fit yields an exponent of $\alpha = 0.94$ and $\alpha = 0.59$ for $\kappa = 0$ and $\kappa = 100$ s^{-1}, respectively, which is in good agreement with the theoretical expectation $\alpha = 1$ for a quantum and $\alpha = 1/2$ for a classical random walk. A quantitative analysis of the decoherence process is provided in Fig. 6(c), where the standard deviation Δx after a fixed propagation time $t_{\text{final}} = 150$ ms is plotted as a function of κ.
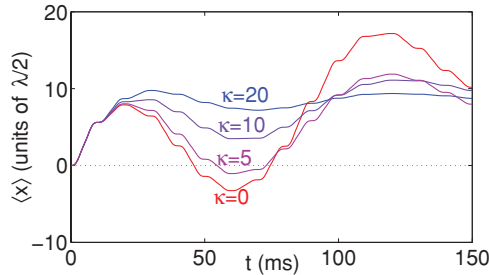
FIG. 7. (Color online) Atomic *Zitterbewegung* in the presence of decoherence. Shown is the position expectation value $\langle x(t) \rangle$ for different values of the dephasing rate κ. Parameters are the same as in Fig. 4 with $\theta = 0.2\pi$.

One observes that Δx decreases with κ until the random walk becomes completely classical at $\kappa \approx 80 \text{ s}^{-1}$.

Also the Dirac quantum simulator discussed in the previous section is vulnerable to decoherence of the atomic hyperfine states. Figure 7 shows an example of the atomic *Zitterbewegung* for the same parameters as in Fig. 4 for different values of the dephasing rate κ. The oscillations of the mean position of the atoms are much less pronounced for $\kappa > 0$. We find that the dephasing rate must not exceed 20 s^{-1} to observe a clear signature of a *Zitterbewegung*. For stronger dephasing no interference effects and thus no oscillations are visible.

VI. CONCLUSION

In the present paper we have explored the rich dynamics of spinor atoms in tilted and driven optical lattices. These systems are nowadays routinely realized experimentally and can be controlled with a high accuracy. We have discussed how a state-dependent transport can be realized by a periodic driving and how this can be used to implement a quantum simulator. A quantum random walk is realized when transitions between the internal states are driven by microwave or Raman pulses. In the continuum limit of weak driving, the dynamics are given by the Dirac equation in a $1 + 1$ dimension. Thus it is possible to investigate relativistic effects such as Zitterbewegung or Klein tunneling in a well-controllable laboratory experiment.

All elements needed for the implementation of the proposed quantum simulator have been demonstrated quite recently such that an experimental realization is possible with current technology. A major obstacle can be decoherence of the internal atomic state. On the other hand, decoherence processes offer the possibility to experimentally study the quantum classical transition for a Dirac particle.

[1] I. Buluta and F. Nori, Science **326**, 108 (2009).

[2] I. Bloch, J. Dalibard, and W. Zwerger, Rev. Mod. Phys. **80**, 885 (2008).

[3] K. S. Novoselov, A. K. Geim, S. V. Morozov, D. Jiang, M. I. Katsnelson, I. V. Grigorieva, S. V. Dubonos, and A. A. Firsov, Nature (London) **438**, 197 (2005).

[4] M. I. Katsnelson, K. S. Novoselov, and A. K. Geim, Nature Phys. **2**, 620 (2006).

[5] L. Lamata, J. León, T. Schätz, and E. Solano, Phys. Rev. Lett. **98**, 253005 (2007).

[6] R. Gerritsma, F. Zähringer, E. Solano, R. Blatt, and C. F. Roos, Nature (London) **463**, 68 (2010).

[7] L. J. Garay, J. R. Anglin, J. I. Cirac, and P. Zoller, Phys. Rev. Lett. **85**, 4643 (2000).

[8] Y. Aharonov, L. Davidovich, and N. Zagury, Phys. Rev. A **48**, 1687 (1993).

[9] M. Karski, L. Förster, J.-M. Choi, A. Steffen, W. Alt, D. Meschede, and A. Widera, Science **325**, 174 (2009).

[10] H. Schmitz, R. Matjeschk, Ch. Schneider, J. Glueckert, M. Enderlein, T. Huber, and T. Schaetz, Phys. Rev. Lett. **103**, 090504 (2009).

[11] A. Schreiber, K. N. Cassemiro, V. Potocek, A. Gabris, P. J. Mosley, E. Andersson, I. Jex, and Ch. Silberhorn, Phys. Rev. Lett. **104**, 050502 (2010).

[12] F. Zähringer, G. Kirchmair, R. Gerritsma, E. Solano, R. Blatt, and C. F. Roos, Phys. Rev. Lett. **104**, 100503 (2010).

[13] S.-L. Zhu, B. Wang, and L.-M. Duan, Phys. Rev. Lett. **98**, 260402 (2007).

[14] J. Otterbach, R. G. Unanyan, and M. Fleischhauer, Phys. Rev. Lett. **102**, 063602 (2009).

[15] E. Haller, R. Hart, M. J. Mark, J. G. Danzl, L. Reichsöllner, and H.-C. Nägerl, Phys. Rev. Lett. **104**, 200403 (2010).

[16] A. Görlitz, T. L. Gustavson, A. E. Leanhardt, R. Löw, A. P. Chikkatur, S. Gupta, S. Inouye, D. E. Pritchard, and W. Ketterle, Phys. Rev. Lett. **90**, 090401 (2003).

[17] M. Gustavsson, E. Haller, M. J. Mark, J. G. Danzl, G. Rojas-Kopeinig, and H.-C. Nägerl, Phys. Rev. Lett. **100**, 080404 (2008).

[18] D. M. Weld, P. Medley, H. Miyake, D. Hucul, D. E. Pritchard, and W. Ketterle, Phys. Rev. Lett. **103**, 245301 (2009).

[19] P. Böhi, M. F. Riedl, J. Hoffrogge, J. Reichl, T. W. Hänsch, and P. Treutlein, Nature Phys. **5**, 592 (2009).

[20] L. Förster, M. Karski, J.-M. Choi, A. Steffen, W. Alt, D. Meschede, A. Widera, E. Montano, J. H. Lee, W. Rakreungdet, and P. S. Jessen, Phys. Rev. Lett. **103**, 233001 (2009).

[21] B. Mischuck, I. H. Deutsch, and P. S. Jessen, Phys. Rev. A **81**, 023403 (2010).

[22] F. Bloch, Z. Phys. **52**, 555 (1929).

[23] J. Feldmann, K. Leo, J. Shah, D. A. B. Miller, J. E. Cunningham, T. Meier, G. von Plessen, A. Schulze, P. Thomas, and S. Schmitt-Rink, Phys. Rev. B **46**, R7252 (1992).

[24] T. Pertsch, P. Dannberg, W. Elflein, A. Bräuer, and F. Lederer, Phys. Rev. Lett. **83**, 4752 (1999).

[25] M. Ben Dahan, E. Peik, J. Reichel, Y. Castin, and C. Salomon, Phys. Rev. Lett. **76**, 4508 (1996).

[26] T. Hartmann, F. Keck, H. J. Korsch, and S. Mossmann, New J. Phys. **6**, 2 (2004).

[27] A. Klumpp, D. Witthaut, and H. J. Korsch, J. Phys. A: Math. Theor. **40**, 2299 (2007).

[28] B. M. Breid, D. Witthaut, and H. J. Korsch, New J. Phys. **8**, 110 (2006).

[29] B. M. Breid, D. Witthaut, and H. J. Korsch, New J. Phys. **9**, 62 (2007).

[30] C. Sias, H. Lignier, Y. P. Singh, A. Zenesini, D. Ciampini, O. Morsch, and E. Arimondo, Phys. Rev. Lett. **100**, 040404 (2008).

[31] A. Zenesini, H. Lignier, D. Ciampini, O. Morsch, and E. Arimondo, Phys. Rev. Lett. **102**, 100403 (2009).

[32] E. Arimondo, M. Inguscio, and P. Violino, Rev. Mod. Phys. **49**, 31 (1977).

[33] F. W. Strauch, Phys. Rev. A **73**, 054302 (2006).

[34] B. Thaller, *The Dirac Equation* (Springer, Berlin, 1992).

[35] J. Dalibard, Y. Castin, and K. Mølmer, Phys. Rev. Lett. **68**, 580 (1992).